

$^{238}\text{U}/^{235}\text{U}$ in calcite is more susceptible to carbonate diagenesis

Xinming Chen^{1,2,3 *}, Stuart A. Robinson⁴, Stephen J. Romaniello⁵, Ariel D. Anbar^{2,6}

¹School of Oceanography, Shanghai Jiao Tong University, Shanghai, 200030, China

²School of Earth & Space Exploration, Arizona State University, Tempe, AZ, 85287, USA

³Department of Earth, Ocean, and Atmospheric Science and National High Magnetic Field

Laboratory, Florida State University, Tallahassee, FL, USA

⁴Department of Earth Sciences, University of Oxford, South Parks Road, Oxford OX1 3AN, UK

⁵Department of Earth and Planetary Sciences, University of Tennessee, Knoxville, TN, 37916,

USA

⁶School of Molecular Sciences, Arizona State University, Tempe, AZ, 85287, USA

(*correspondence: xchen6@sjtu.edu.cn)

Abstract

The uranium isotopic composition ($\delta^{238}\text{U}$) of bulk marine calcium carbonates has been extensively explored as a promising paleoredox proxy to track the extent of global oceanic anoxia in deep time. Multiple studies have examined whether primary calcium carbonates can directly capture seawater $\delta^{238}\text{U}$ and whether bulk measurements of recent and ancient carbonates preserve seawater U isotope signatures. Here we assess the role of diagenesis in altering $\delta^{238}\text{U}$ signatures in carbonates sediments that have a primary calcitic mineralogy at the Paleocene-Eocene Thermal Maximum (PETM), an interval with rapid global warming and oceanic deoxygenation at ~56 million years ago.

Although primary abiotic and biogenic calcium carbonates (aragonite and calcite) can directly capture seawater $\delta^{238}\text{U}$ with small offsets ($< 0.1\text{‰}$) relative to modern seawater, diagenetic alteration of Bahamian shallow-water platform carbonate sediments that have a predominantly primary aragonitic mineralogy resulted in significantly larger offsets (up to 0.6‰). Since U concentration in aragonite is at least one order of magnitude higher than calcite ($> 1\text{ ppm}$ vs. $< 0.1\text{ ppm}$), $\delta^{238}\text{U}$ in calcite should be even more susceptible to diagenesis than that in aragonite.

We find strong evidence of this effect in analysis of $\delta^{238}\text{U}$ in PETM shallow-water carbonate sediments from Drilling Project (ODP) Hole 871C (Limalok Guyot, Pacific Ocean). Our results reveal large fluctuations in bulk carbonate $\delta^{238}\text{U}$ from -0.69 to $+0.71\text{‰}$ around the PETM boundary but consistently heavier $\delta^{238}\text{U}$ (between -0.14 and $+0.47\text{‰}$) than modern seawater outside of this interval. The significantly lighter $\delta^{238}\text{U}$ values than modern seawater were interpreted to result from the operation of a Mn oxide shuttle. The heavier $\delta^{238}\text{U}$ values are most likely caused by authigenic reductive accumulation of U(IV) in pore waters below the sediment-water interface. We found that carbonate $\delta^{238}\text{U}$ values higher than modern seawater tend to

increase with increasing U/Ca. This relationship is well-explained by an authigenic reductive accumulation model that simply assumes addition to primary calcite during diagenesis of calcitic cements containing isotopically heavier U(IV).

Our work confirms expectations that $\delta^{238}\text{U}$ in primary calcite is more susceptible to the amount of diagenetic cementation compared to primary aragonite, and that variations of $\delta^{238}\text{U}$ in carbonate sediments with a primary calcitic mineralogy would more dominantly reflect the local redox state of depositional and early diagenetic environments. It is essential to identify the original carbonate mineralogy, the diagenetic history, and constrain the redox state of local deposition environments of sedimentary carbonate rocks when applying bulk carbonate $\delta^{238}\text{U}$ as a global proxy for oceanic anoxia in deep time.

Keywords: U isotopes; calcite and aragonite; paleoredox proxy; diagenesis; local and global

1. Introduction

Reconstructing Earth's oxygenation history is key to our understanding of the evolution of life because the rise and fall of atmospheric oxygen through time strongly affects, and is affected by, the biosphere (e.g., Fenchel and Finlay, 1994; Berner et al., 2007; Lyons et al., 2014). For example, the emergence and evolution of early animal life in the Late-Neoproterozoic was associated with the oxygenation of the atmosphere and oceans, whereas the three major mass extinction events of the Phanerozoic—in the Late Devonian, end-Permian, and end-Triassic—coincided with oceanic anoxia (e.g., Canfield et al., 2007; Berner et al., 2007; Mills et al., 2014; Reinhard et al., 2016). These intimate links indicate that it is crucial to reconstruct Earth's oxygenation history to unravel the co-evolution of life and Earth.

Multiple geochemical proxies can be used to reconstruct Earth's oxygenation history from a wide range of sedimentary rock types, including the abundance of redox-sensitive elements (e.g., V, Mo, Re, U, Cr, I/Ca), and the stable isotopic composition of light elements ($\delta^{13}\text{C}$, $\delta^{15}\text{N}$, $\delta^{34}\text{S}$) and heavy elements ($\delta^{56}\text{Fe}$, $\delta^{53}\text{Cr}$, $\delta^{51}\text{V}$, $\delta^{82}\text{Se}$, $\delta^{98}\text{Mo}$, $\epsilon^{205}\text{Tl}$, $\delta^{238}\text{U}$) (e.g., Anbar and Rouxel, 2007; Lyons et al., 2009; Pufahl and Hiatt, 2012; Fan et al., 2021; Lu et al., 2010). Among these paleoredox proxies, variations of $\delta^{238}\text{U}$ in sedimentary carbonate rocks are being explored as a novel tool to track the global redox conditions of oceans through time (e.g., Brennecke et al., 2011a; Lau et al., 2016; del Rey et al., 2020; Clarkson et al., 2021; Song et al., 2017; White et al., 2018; Elrick et al., 2017; Cheng et al., 2020; Wei et al., 2018; Zhang et al., 2018; Gilleaudeau et al., 2019; Tostevin et al., 2019). Uranium isotopic mass balance in modern oceans demonstrates that seawater $\delta^{238}\text{U}$ is driven by variations in ocean redox conditions (Andersen et al., 2017; Weyer et al., 2008). Uranium in the oceans mainly comes from continental weathering, with negligible isotope fractionation (Andersen et al., 2015, 2017; Tissot and Dauphas, 2015; Weyer et al., 2008).

Marine U is mainly removed by reduction of dissolved U(VI) as insoluble U(IV), adsorption to Fe and Mn oxides (e.g., ferromanganese crust and nodules), coprecipitation with calcium carbonates, and hydrothermal alteration (Dunk et al., 2002). Among these U removal processes, U reduction is the most efficient pathway and causes the largest isotope fractionation $\sim 1\text{‰}$ (Andersen et al., 2015, 2017; Tissot and Dauphas, 2015; Weyer et al., 2008). Hence, seawater $\delta^{238}\text{U}$ is predominantly driven by the redox conditions of the oceans. Since U has a relatively long residence time (~ 500 kyr), compared to the ocean mixing time (~ 2 kyr, Dunk et al., 2002; Ku et al., 1977), $\delta^{238}\text{U}$ at any location of the open oceans should be homogeneous, reflecting the average global redox state. If U isotopes in marine calcium carbonates capture and preserve the coeval seawater U isotopic composition, then $\delta^{238}\text{U}$ in carbonate rocks can be used to reconstruct the global redox conditions of ancient oceans. The robustness of this paleoredox proxy relies heavily on this assumption.

Multiple studies have explored the reliability of this proxy by examining two questions: (1) whether primary abiotic and biogenic calcium carbonates can directly capture coeval seawater U isotopic composition, and (2) whether bulk carbonate sediments can preserve the original $\delta^{238}\text{U}$ in primary calcium carbonates during diagenesis. Laboratory experiments and field work revealed small or negligible isotope fractionations ($< 0.10\text{‰}$) in primary calcium carbonates (Chen et al., 2016, 2018a; Livermore et al., 2020), answering the first question. Calcium carbonate coprecipitation experiments demonstrated a small isotope fractionation of $\sim 0.10\text{‰}$ during U(VI) incorporation into abiotic aragonite but not calcite under pH ~ 8.5 (Chen et al., 2016). Field work also revealed that biological effects can cause variable U isotope fractionation ($0 - 0.09\text{‰}$) during U uptake by primary biogenic calcium carbonates such as ooids, stromatolites, corals, red and green calcareous algae, microbial calcite, and brachiopods (Chen et al., 2018a, 2021; Romaniello

et al., 2013; Weyer et al., 2008; Stirling et al., 2007; Andersen et al., 2016; Tissot and Dauphas, 2015; Livermore et al., 2020). Briefly, precipitation of primary abiotic and biogenic calcium carbonates can directly capture seawater $\delta^{238}\text{U}$ with small or little isotopic offsets of less than 0.10‰.

In contrast, diagenesis has been demonstrated to significantly impact, to varying degrees, $\delta^{238}\text{U}$ in bulk carbonate sediments compared to $\delta^{238}\text{U}$ of primary calcium carbonates. Modern carbonate sediments deposited under anoxic bottom waters record significant U isotopic offsets from water column values. Recent work revealed a U isotopic offset of $\sim +0.6\text{‰}$ (relative to bottom waters) in carbonate sediments derived from microbial calcite that were deposited beneath sulfidic bottom waters, in the modern redox-stratified lake Fayetteville Green Lake (New York, USA) (Chen et al., 2021). This finding reflects the typical U isotope fractionation observed in other modern organic-rich sediments deposited under anoxic bottom waters (Andersen et al., 2014, 2017). Anoxic deposition was also suggested to cause isotopic offsets of 0.4 – 0.6‰ (relative to coeval seawater) in Paleocene-Eocene deep-sea pelagic carbonates that were originally foraminiferal calcite (Clarkson et al., 2021). Anoxic depositional environments typically result in reduction of dissolved U(VI) in anoxic water columns and pore waters below the sediment-water interface, leading to significant sedimentary authigenic enrichments of isotopically heavier U(IV) (> 10 ppm, e.g., Partin et al., 2013). Since U in primary biogenic calcite is typically low (0.2 – 30 ppb; e.g., Russell et al., 2004; Chen et al., 2018a, 2020; Keul et al., 2013; Allen et al., 2016), the anoxic deposition of authigenic carbonate sediments can easily overprint the original $\delta^{238}\text{U}$ in primary calcite grains.

Modern Bahamian shallow-water platform carbonate sediments (predominantly aragonitic mineralogy) deposited under oxic bottom waters with reducing pore waters also record carbonate

$\delta^{238}\text{U}$ values higher than modern seawater ($-0.14 \pm 0.15\text{‰}$, $N = 162$, 1σ , vs. seawater = $-0.392 \pm 0.005\text{‰}$) (Romaniello et al., 2013; Chen et al., 2018b, 2020; Tissot and Dauphas, 2015; Tissot et al., 2018; Russell et al., 2004). The positive isotope offsets in these carbonate sediments were interpreted to result from authigenic reductive accumulation of U(IV), by a concentration of $\sim 2.5 \pm 1$ ppm, below the sediment-water interface. The concentration of U(IV) in these shallow-water carbonates, derived authigenically during diagenesis, is at least two orders of magnitude higher than the U concentration in primary calcite precipitates (0.2 – 30 ppb, e.g., Russell et al., 2004; Chen et al., 2018a, 2020; Keul et al., 2013; Allen et al., 2016), suggesting that $\delta^{238}\text{U}$ in carbonate sediments with a primary calcitic mineralogy should be more easily offset from seawater $\delta^{238}\text{U}$, compared to carbonate sediments with a primary aragonitic mineralogy which typically have significantly higher U concentrations at least one order of magnitude higher than calcite (e.g., Reeder et al., 2000; Keul et al., 2013; Romaniello et al., 2013).

To explore the potential effects of diagenesis on shallow-water carbonate sediments deposited beneath oxic bottom waters with a primary calcitic mineralogy, we collected samples from a Paleogene carbonate platform succession recovered from Limalok Guyot (Pacific Ocean) at Ocean Drilling Project (ODP) Site 871. Bulk carbonate samples were measured for trace element and rare earth element concentrations and $\delta^{238}\text{U}$ values. Our results documented positive U-isotopic offsets ($\sim 0.5 - 1.2\text{‰}$ relative to coeval seawater) that increased with U/Ca and negative isotopic offsets ($\sim 0.2\text{‰}$) that might be associated with a Mn oxide shuttle.

2. Samples

Our geochemical data are derived from ODP Site 871 on Limalok Guyot in the Pacific Ocean, drilled during ODP Leg 144 (Premoli-Silva et al., 1993). At Hole 871C, ~ 300 m of a

Paleogene carbonate platform (from 133.7 to 422.9 meters below seafloor (mbsf)) overlying a volcanic edifice was cored (Premoli Silva et al., 1993; Watkins et al., 1995; Wilson et al., 1998). Carbonates from Hole 871C primarily consist of benthic foraminiferal packstone/wackestone, miliolid-intraclast grainstone, and rohodolith grain/packstone, which have a predominantly primary calcitic mineralogy (Premoli Silva et al., 1993; Ogg et al., 1995; Scholle and Ulmer-Scholle, 2003). Shipboard analyses indicate that the shallow-water carbonates from Hole 871C have calcium carbonate contents of 95 – 98% and contain less than 0.3% organic carbon and no sulfur (Premoli Silva et al., 1993).

Previous work on the shallow-water carbonate sediments from Hole 871C has explored the diagenetic and stratigraphic history in some detail. On the basis of petrography and stable-isotopic geochemistry, Wyatt et al. (1995) concluded that most of the diagenetic alteration and cementation occurred in the marine realm, largely during early marine diagenesis (rather than meteoric or burial diagenesis). The existence of some limited intervals with well-developed moldic and vuggy porosity and light oxygen isotope values was taken to indicate some possible meteoric diagenesis, although classic indicators (such as vadose-zone cements and depleted $\delta^{13}\text{C}_{\text{carb}}$ values) have not been reported. Robinson (2011) used high-resolution stable-isotope measurements and biostratigraphy to argue for the existence of a partial record of the Paleocene-Eocene Thermal Maximum (PETM) in Hole 871C.

Twenty-nine samples from Hole 871C were selected for $\delta^{238}\text{U}$ characterization, from 150 to 420 mbsf which covers the approximate time interval 46 – 58 Ma (based on the age model of Robinson, 2011). We sampled carbonates at high-resolution over the Paleocene-Eocene Thermal Maximum (PETM) interval (335.80 – 336.30 mbsf) and earliest Eocene (321.21 – 326.42 mbsf)

to see if we could capture any variations in seawater $\delta^{238}\text{U}$ related to global oceanic deoxygenation during that event that were preserved despite diagenesis.

3. Methods

3.1 Trace metal and rare earth elements concentration analysis

For each sample, about two grams of carbonate were powdered and homogenized using a ball mill equipped with silicon carbide mortars. Then, approximately 0.5 – 1 g powdered carbonate sediments from each sample were leached with 1 M trace-metal grade nitric acid overnight to extract the fraction of U associated with carbonates. The resulting solutions were then centrifuged at 4500 rpm for 30 min to remove insoluble solids. A small aliquot of the supernatant was diluted in 2% nitric acid for the measurement of trace element and rare earth element (REE) concentrations on a Thermo iCAP Q inductively coupled plasma mass spectrometer (ICP-MS) at W. M. Keck Foundation Laboratory for Environmental Biogeochemistry, Arizona State University. The cerium anomaly (Ce/Ce^*) is calculated based on its geometric average relative to its neighbor elements Pr and Nd (e.g., Ling et al., 2011; Tostevin et al., 2016) and normalized to the average Post-Archean Australian shale (PAAS) using the equation:

$$\text{Ce}/\text{Ce}^* = \text{Ce} \times \text{Pr}/\text{Nd}^2 \quad (1)$$

3.2 Uranium isotope analysis

Based on the measured trace element concentration data, approximately 250 ng U was taken from each sample and spiked with a ^{233}U - ^{236}U double-spike (IRMM-3636) at a $\text{U}_{\text{spike}}:\text{U}_{\text{sample}}$ ratio of 0.0363 (Verbruggen et al., 2008). These sample solutions were digested with aqua regia and conc. $\text{HNO}_3 + 30\% \text{H}_2\text{O}_2$ to removal organic matter. The digested samples were dissolved in 3 M HNO_3 for purification of U by chromatographic column chemistry.

Purification of U followed the Eichrom UTEVA resin procedure (Chen et al., 2016a; Weyer et al., 2008). Briefly, ~ 1 ml UTEVA resin (Eichrom Technologies, LLC) was loaded into 10 ml chromatography columns (Bio-Rad Laboratories, Inc.), and rinsed with 2.5 ml 0.05 M HCl four times to remove any U induced during the loading step. Then, the resin was conditioned with 3 × 1 ml 3 M HNO₃. Samples (dissolved in 3 M HNO₃) were load onto the columns and washed with 15 ml 3 M HNO₃ to clean all the matrix ions except U and Th. Following this, the resin was rinsed with 10 M HCl (3 × 1 ml) to convert it to chloride form. Th on the resin was then removed using 5 M HCl + 0.05 M oxalic acid (3 × 0.8 ml). The oxalic acid left on the resin was cleaned using 5 M HCl (3 × 1 ml). Finally, U adsorbed to the UTEVA was eluted using 0.05 M HCl (~7 ml). The eluted U cuts were dried down and digested with conc. HNO₃ + 30% H₂O₂ to get rid of organic residue eluted from the UTEVA resin.

After purification, U isotopic ratios were measured at a U concentration of ~50 ppb in 2% trace metal clean nitric acid on a Thermo Scientific Neptune MC-ICP-MS equipped with an ESI Apex desolvating nebulizer at ASU (W. M. Keck Foundation Laboratory for Environmental Biogeochemistry, Arizona State University). Ion beams of ²³³U, ²³⁵U, ²³⁶U and ²³⁸U were collected with Faraday cups connected to 10¹¹ Ω, 10¹¹ Ω, 10¹¹ Ω, 10¹⁰ Ω resistors. The signal for ²³⁸U from a 50 ppb U solution was ~ 30 volts. Uranium isotopic composition was reported in δ notation in per mil (‰) relative to the U reference standard CRM-145a:

$$\delta^{238}\text{U} = \left[\frac{\left(\frac{^{238}\text{U}}{^{235}\text{U}} \right)_{\text{sample}}}{\left(\frac{^{238}\text{U}}{^{235}\text{U}} \right)_{\text{CRM-145a}}} - 1 \right] \times 1000 \quad (2)$$

At least three replicate measurements were performed for each sample. The uncertainty in $\delta^{238}\text{U}$ was reported as twice the standard deviation of either the sample or the standard CRM-145a.

The blank for the U column chemistry was < 0.05 ng. The reproducibility of the repeated measurements of $\delta^{238}\text{U}$ in CRM-145a was $\pm 0.08\text{‰}$ (2 SD, N = 45). The accuracy of U isotope analysis was monitored by analyzing the secondary standard CRM-129a. The average $\delta^{238}\text{U}$ value for this standard was $-1.79 \pm 0.08\text{‰}$ (2 SD, N = 25), in good agreement with previous published data ($-1.70 \pm 0.08\text{‰}$ and $-1.72 \pm 0.10\text{‰}$ (2 SD); Chen et al., 2018b; Wang et al., 2015).

4. Results

4.1 Concentration of redox-sensitive elements and Ce anomaly

The shallow-water carbonates in Hole 871C documented different extents of enrichments of redox-sensitive elements (“RSE”) V, Mo, Re, and U (Fig. 2A – D; see Table S1 in Supplementary information). The leached carbonate fraction from each sample contained an undetectable amount of Al and Th (see Table S1 in Supplementary information). As a result, we infer that the concentrations of RSE measured in our acid-leached samples include negligible contributions from detrital materials. Vanadium concentration varied between 1 and 30 ppm, increased to up to 70 ppm over the PETM interval (317 – 336 mbsf defined by Robinson, 2011), and decreased back to < 30 ppm above 336 mbsf. Both Mo (< 0.1 ppm) and Re (< 3 ppb) concentrations remained relatively low and invariant beyond the PETM interval with occasionally one and two data points of high concentrations of Mo (~ 2 ppm) and Re (4 and 7 ppb). Uranium concentration below the boundary varied between 0.2 and 5 ppm, elevated up to 18 ppm over the interval, and immediately decreased back to < 4 ppm. The cerium anomaly (Ce/Ce^*) was consistently < 0.5 throughout the whole carbonate section (see the rare earth elements (REEs) data and full REE pattern in Table S1 and Figure S1, respectively, in the supplementary material).

4.2 Bulk carbonate $\delta^{238}\text{U}$ from ODP Hole 871C

Bulk shallow-water carbonate $\delta^{238}\text{U}$ from ODP Hole 871C is generally heavier than the reported Paleocene-Eocene seawater (-0.36‰ ; Clarkson et al., 2021) varying between -0.14 and 0.47‰ , except during the PETM interval and lowermost Eocene, from which bulk carbonate $\delta^{238}\text{U}$ fluctuate significantly between -0.69 to $+0.71\text{‰}$ (Fig. 3D; see Table 1). In detail, $\delta^{238}\text{U}$ values decrease continuously from $+0.71$ to -0.53‰ between 336.30 and 335.80 mbsf (Fig. 3E) while they increase progressively from -0.73 to -0.46‰ between 326.42 to 326.26 mbsf except for one data point with a positive value of 0.46‰ (Fig. 3E).

5. Discussion

Our data document $\delta^{238}\text{U}$ values lighter than modern seawater over the PETM to lower Eocene interval, and consistently higher $\delta^{238}\text{U}$ values ($> -0.39\text{‰}$) beyond this interval. To interpret these U isotope data, we first constrain the seawater $\delta^{238}\text{U}$ over the Paleocene-Eocene and the redox state of local depositional environments. Then, we explore the possible mechanisms that cause the lighter and higher $\delta^{238}\text{U}$ values in ODP Hole 871C. Finally, we discuss the implications of bulk carbonate $\delta^{238}\text{U}$ as a paleoredox proxy to infer global redox conditions of oceans in deep time.

5.1 Seawater $\delta^{238}\text{U}$ over the Paleocene-Eocene

To explore the effects of diagenesis on U isotopes in Paleocene-Eocene carbonate sediments, it is essential to constrain coeval seawater $\delta^{238}\text{U}$, which is predominantly controlled by the global redox state of the oceans. Measurements of U isotopes in ferromanganese crusts revealed an invariant isotopic offset of -0.24‰ from modern seawater, suggesting that seawater

$\delta^{238}\text{U}$ did not change over the Cenozoic (Wang et al., 2016). High-resolution profiles of pelagic carbonate $\delta^{238}\text{U}$ data over the PETM suggested a limited expansion of oceanic anoxia and that Paleocene-Eocene seawater had a $\delta^{238}\text{U}$ value of -0.36‰ (Clarkson et al., 2021), very close to modern seawater $\delta^{238}\text{U}$ ($-0.392 \pm 0.005\text{‰}$; Tissot et al., 2015). The limited expansion of oceanic anoxia is supported by a cGENIE model result that suggests anoxia/dysoxia rose by 2% to reach 4% of the global ocean volume during the transition from pre-PETM to PETM (Rommelzwaal et al., 2019). For simplicity, we assume that Paleocene-Eocene seawater $\delta^{238}\text{U}$ remained invariant around -0.39‰ .

5.2 Redox state of local depositional environments for ODP Hole 871C

Previous studies revealed that the redox state of local depositional environments significantly affects $\delta^{238}\text{U}$ measured in bulk carbonate sediments. Specifically, carbonate sediments deposited under reducing bottom waters exhibited profound enrichments in U concentration, and consistently higher $\delta^{238}\text{U}$ values than coeval seawater (Chen et al., 2021; Clarkson et al., 2021). In contrast, carbonate sediments deposited under oxic bottom waters resulted in little to large increases in U content and $\delta^{238}\text{U}$, dominantly depending on the amount of pore water U(VI) reduction (Romaniello et al., 2013; Chen et al., 2018; Tissot et al., 2018; Clarkson et al., 2021). Thus, we first investigate the redox state of local depositional environments of ODP Hole 871C prior to discussion of the carbonate $\delta^{238}\text{U}$ data.

Our Ce anomaly and RSE data suggest that carbonates from Hole 871C were deposited under oxic bottom waters with anoxic (but generally non-euxinic) pore waters below the sediment-water interface. The Ce/Ce^* was consistently lower than 0.5 throughout the whole carbonate section, indicating that these carbonates were deposited under oxic bottom waters and pore waters

(Haley et al., 2004). In contrast, the concentrations of V and Re in Hole 871C were moderately higher than in primary biogenic calcium carbonates (1 – 70 ppm vs. 0.01 – 0.5 ppm for V and 1 – 7 ppb vs. <1 ppb for Re; Chen et al., 2018a; Romaniello et al., 2013), implying at least reducing pore waters below the sediment-water interface. Like V and Re, Hole 871C also documented significant enrichments of U, particularly over the PETM interval (~320 – 327 mbsf). The very low Mo concentrations in carbonates from Hole 871C (compared to primary biogenic carbonates 0.01 – 0.1 ppm; Romaniello et al., 2016), on the other hand, suggest that the pore waters were non-euxinic. It should be noted that V, Mo, and U concentrations were the highest (67 ppm, 1.8 ppm, and 18.3 ppm) at 326.37 mbsf, suggesting likely euxinic pore waters.

5.3 Alteration of $\delta^{238}\text{U}$ during carbonate diagenesis

5.3.1 Negative $\Delta^{238}\text{U}$ associated with a Mn oxide shuttle

The lighter carbonate $\delta^{238}\text{U}$ values between -0.47‰ and -0.69‰ over the PETM boundary (Fig. 4) are most likely associated with organic matter and manganese (Mn) oxides, rather than the expansion of global oceanic anoxia. Although multiple geochemical proxies ($\delta^{34}\text{S}$ in barite, I/Ca and $\delta^{53}\text{Cr}$ in foraminifera, and abundances of Mn and U in carbonates) indicated heterogeneous oceanic deoxygenation over the PETM (Yao et al., 2018; Zhou et al., 2014, 2016; Chun et al., 2010; Remmelzwaal et al., 2019), the extent of global oceanic anoxia cannot cause the extremely light carbonate $\delta^{238}\text{U}$ values (-0.63‰ and -0.69‰) observed in ODP Hole 871C. These light U isotopic compositions are similar to $\delta^{238}\text{U}$ values ($\sim -0.7\text{‰}$) in carbonates of the end-Permian mass extinction interval (Brennecke et al., 2011; Lau et al., 2016; Zhang et al., 2018). The light end-Permian carbonate $\delta^{238}\text{U}$ values were interpreted to result from an expansion of the anoxic seafloor to 20%. If our light carbonate $\delta^{238}\text{U}$ values over PETM interval in ODP Hole 871C

were also caused by an expansion of oceanic anoxia, the predicted anoxic seafloor area would be ~ 20%. This prediction is inconsistent with Paleocene-Eocene pelagic carbonate $\delta^{238}\text{U}$ values that suggested a maximum expansion of anoxic seafloor area to ~ 2% (Clarkson et al., 2021) as well as cGENIE model results which inferred that only 4% of the global ocean volume was anoxic over the PETM (Rommelzwaal et al., 2019). Furthermore, the high-resolution profiles of $\delta^{238}\text{U}$ over the PETM interval (317 – 326 mbsf, Fig. 3E) revealed significant and abrupt fluctuations of carbonate $\delta^{238}\text{U}$ between –0.69‰ and +0.71‰ within a short time period of less than 200 kyr, conflicting with the lack of resolvable perturbation to the U cycle over this short time period (Clarkson et al., 2021).

Alternatively, our lighter carbonate $\delta^{238}\text{U}$ values could be the consequence of an association with organic matter or Mn oxides. Organic matter preferentially uptakes ^{235}U with an isotope fractionation of ~0.2‰, and uptake by organic matter has been proposed to explain the shift of $\delta^{238}\text{U}$ in Paleocene-Eocene pelagic carbonates and modern organic-rich marine sediments to values lighter than coeval seawater (Chen et al., 2020; Clarkson et al., 2021; Abshire et al., 2019). Among all published U isotope data, only two modern organic-rich sediment samples (total organic carbon (TOC) = 8 and 9 wt%) from the anoxic shelf of Namibia had lighter $\delta^{238}\text{U}$ values (–0.59 and –0.62‰) with high authigenic U concentrations of 5 and 10 ppm. However, the extremely low TOC content (less than 0.3 wt%; Premoli Silva et al., 1993) in our samples from Hole 871C cannot result in the accumulation of the high U concentrations of ~ 4 – 6 ppm, ruling out the effects of organic matter on our $\delta^{238}\text{U}$ data.

Experimental studies also demonstrated that Mn oxides preferentially adsorb ^{235}U , with an isotope fractionation of ~ 0.2‰ (Brennecka et al., 2011b; Dang et al., 2016; Jemison et al., 2016). The ~ 0.24‰ isotopic offset between carbonate $\delta^{238}\text{U}$ and coeval seawater at this depth is

consistent with that observed during U(VI) adsorption to Mn-oxides (Brennecke et al., 2011b; Dang et al., 2016; Jemison et al., 2016). A minor amount of pore-lining Mn oxide observed at a depth of ~317 mbsf of ODP Hole 871C (Wyatt et al., 1995) supports the argument that Mn oxides most likely lead to lighter carbonate $\delta^{238}\text{U}$ than coeval seawater. It should be noted that these carbonate sediments have relatively high U concentrations, ~ 7 to 10 ppm. Manganese oxides affect carbonate $\delta^{238}\text{U}$, likely via a particulate Mn-shuttle proposed by Herrmann et al. (2018). The operation of a particulate Mn-shuttle can significantly increase U concentration but decrease $\delta^{238}\text{U}$ in carbonate sediments. Our redox-sensitive element concentrations and Ce/Ce* data suggest a redoxcline below the sediment-water interface, favoring the active operation of a particulate Mn-shuttle (Algeo and Tribovillard, 2009). The reducing but non-sulfidic pore waters below the sediment-water interface (see Section 5.2) would dissolve Mn oxides, releasing soluble Mn back to bottom waters but scavenging the U sorbed to Mn oxides via reduction of U(VI) to insoluble U(IV).

5.3.2 Positive $\Delta^{238}\text{U}$ induced by authigenic reduction of U(IV) in pore waters

Diagenetic alteration of carbonate sediments at ODP Hole 871C leads to higher carbonate $\delta^{238}\text{U}$ values in bulk carbonate sediment relative to values expected for primary biogenic calcite grains (i.e., benthic foraminifera, echinoderms, and calcareous red algae) and in comparison to modern seawater (Fig. 5a). The isotopic offset between carbonate sediments and Paleogene seawater ($\Delta^{238}\text{U}$) is $0.59 \pm 0.24\text{‰}$ (N = 24, 1 σ). The magnitude of this offset is significantly larger than the offset observed between Bahamian carbonate sediments that have a predominantly primary aragonitic mineralogy and modern seawater (Fig. 5b; $\Delta^{238}\text{U} = 0.25 \pm 0.15\text{‰}$, N = 162, 1 σ ; Romaniello et al., 2013; Chen et al., 2018b; Tissot et al., 2018; Chen et al., 2018a; Livermore

et al., 2020). Furthermore, it is also observed that carbonate sediments from Hole 871C with positive $\Delta^{238}\text{U}$ values show a positive correlation between increased $\delta^{238}\text{U}$ values and U/Ca (Spearman's correlation coefficient: $\rho = 0.47$, $p\text{-value} = 0.02$, Fig. 4).

Since carbonate sediments from Hole 871C were deposited under oxic bottom waters, the existence of carbonate $\delta^{238}\text{U}$ values higher than modern seawater (Fig. 4) likely results from authigenic reductive accumulation of U(IV) in pore waters below the sediment-water interface during early diagenesis. Consistent with previous work on shallow-water platform carbonate sediments from the Bahamas (Chen et al., 2018b; Tissot et al., 2018), the significantly higher U concentrations in carbonate sediments in ODP Hole 871C compared to primary biogenic calcite precipitates (0.1 – 18 ppm vs. 0.01 – 0.11 ppm) likely results from dramatic authigenic enrichments of U(IV) during carbonate diagenesis. These authigenic phases containing U(IV), which preferentially accumulates ^{238}U during U(VI) reduction, could lead to higher bulk carbonate $\delta^{238}\text{U}$ values compared to primary calcite grains. The 10- to 100-fold enrichments of authigenic U(IV) and significantly larger U isotope fractionation during U(VI) reduction to U(IV) than calcite coprecipitation with U(VI) (0.4 – 1.2‰ vs. 0 – 0.1‰; Basu et al., 2014; Stirling et al., 2015; Sytlo et al., 2015; Brown et al., 2018; Andersen et al., 2017; Chen et al., 2016, 2017, 2018a) can easily overprint the coeval seawater $\delta^{238}\text{U}$ signals in biogenic calcites through the addition of cements during early diagenesis. Hence, we suggest that bulk carbonate $\delta^{238}\text{U}$ values from Hole 871C (excluding samples with lighter $\delta^{238}\text{U}$ values than coeval seawater) are predominantly controlled by the amount of authigenic U(IV), and so follow a general increasing trend with U/Ca.

5.3.3 An authigenic U accumulation model for positive $\Delta^{238}\text{U}$ in ODP Hole 871C

To explore the effects of authigenic reduction of U(VI) in pore water below the sediment-water interface on carbonate $\delta^{238}\text{U}$ during diagenesis, we establish a simple geochemical model to interpret the covariation of carbonate $\delta^{238}\text{U}$ with U/Ca. This model assumes: (1) little or negligible calcite dissolution and recrystallization occurred, due to the stability of primary calcite grains in seawater; (2) reductive accumulation of U(IV) in pore waters below the sediment-water interface during early diagenetic precipitation of calcite cements predominantly causes U isotope fractionation during diagenesis; (3) U(VI) is incorporated into primary biogenic calcite with little isotope fractionation (Fig. 6A; Chen et al., 2016, 2017, 2018a; Livermore et al., 2020). Under these assumptions, carbonate $\delta^{238}\text{U}$ in bulk carbonate sediments ($\delta^{238}\text{U}_{\text{carb}}$) is, thus, determined by the relative fractions of primary carbonate U (f_{primary}) and authigenic U(IV) (f_{auth}) added during diagenesis. The $\delta^{238}\text{U}$ value in the bulk carbonate sediments can be estimated by:

$$\delta^{238}\text{U}_{\text{carb}} = f_{\text{auth}} \times \delta^{238}\text{U}_{\text{auth}} + (1 - f_{\text{primary}}) \times \delta^{238}\text{U}_{\text{primary}} \quad (3)$$

where $\delta^{238}\text{U}_{\text{primary}}$ and $\delta^{238}\text{U}_{\text{auth}}$ are isotopic compositions of U in primary calcium carbonate precipitates and authigenic U(IV) in carbonate sediments, respectively. Since U isotope fractionation during primary calcium carbonate precipitation is little or negligible ($< 0.1\text{‰}$; Chen et al., 2018a; Livermore et al., 2020), $\delta^{238}\text{U}_{\text{primary}}$ ($= -0.39\text{‰}$) equals that of coeval seawater ($\delta^{238}\text{U}_{\text{sw}}$). Also, the isotopic composition of authigenic U(IV) can be described by:

$$\delta^{238}\text{U}_{\text{auth}} = \delta^{238}\text{U}_{\text{sw}} + \Delta^{238}\text{U}_{\text{auth-sw}} \quad (4)$$

where $\Delta^{238}\text{U}_{\text{auth-sw}}$ is the isotope fractionation during U(VI) reduction to U(IV). Substituting Eq. 4 into Eq. 3, we can obtain

$$\delta^{238}\text{U}_{\text{carb}} = (1 - f_{\text{primary}}) \times \Delta^{238}\text{U}_{\text{auth-sw}} + \delta^{238}\text{U}_{\text{primary}} \quad (5)$$

The fraction of primary carbonate U in bulk carbonate sediments can be estimated as:

$$f_{\text{primary}} = \frac{\left(\text{U/Ca}\right)_{\text{primary}}}{\left(\text{U/Ca}\right)_{\text{carb}}} \quad (6)$$

382 Substituting Eq. 6 into Eq. 5, we can obtain

$$\delta^{238}\text{U}_{\text{carb}} = \left[1 - \frac{\left(\text{U/Ca}\right)_{\text{primary}}}{\left(\text{U/Ca}\right)_{\text{bulk}}} \right] \times \Delta^{238}\text{U}_{\text{auth-sw}} + \delta^{238}\text{U}_{\text{primary}} \quad (9)$$

383 Equation 9 reveals that carbonate $\delta^{238}\text{U}$ in bulk carbonate sediments depends on the relative
 384 fraction of authigenic U(IV) (f_{IV} defined in Eq. 8) and the magnitude of isotope fractionation
 385 ($\Delta^{238}\text{U}_{\text{auth-sw}}$) during authigenic reduction of U(VI) to U(IV). Since ODP Hole 871C (this study)
 386 and coeval pelagic carbonates (ODP sites 690, 401, and 865 from Clarkson et al. (2021)) have a
 387 predominantly primary calcitic mineralogy, we assume carbonates with $\delta^{238}\text{U}$ close to
 388 contemporaneous seawater preserve the Paleocene-Eocene primary calcite U/Ca, ranging from ~
 389 0.02 to 0.10 $\mu\text{mol/mol}$ (Fig. 6A), which is higher than U/Ca in foraminiferal calcite in modern
 390 oceans (e.g., 0.01 – 0.02 $\mu\text{mol/mol}$; Keul et al., 2013). The higher U/Ca in these Paleocene-Eocene
 391 foraminiferal calcite likely results from the significantly lower seawater $[\text{CO}_3^{2-}]$ in Paleocene-
 392 Eocene seawater relative to modern oceans (~100 $\mu\text{mol/mol}$ vs. ~200 $\mu\text{mol/mol}$; Zeebe and Tyrrell,
 393 2019). The U/Ca in foraminiferal calcite is predominantly controlled by seawater chemistry and
 394 increases significantly with seawater $[\text{CO}_3^{2-}]$ (Russell et al., 2004; Allen et al., 2016; Keul et al.,
 395 2013; Chen, 2020). The $\Delta^{238}\text{U}_{\text{auth-sw}}$ during abiotic and biotic U(VI) reduction varied between 0.4
 396 to 1.2‰, depending on the U reduction kinetics and aqueous U speciation (Basu et al., 2014, 2020;
 397 Brown et al., 2018; Wang et al., 2015; Stylo et al., 2015; Stirling et al., 2015).

398 According to our model, the predicted range of carbonate $\delta^{238}\text{U}$ (gray area in Fig. 6A)
 399 during diagenesis can cover nearly all the $\delta^{238}\text{U}$ values ($> -0.39\text{‰}$) in Paleocene-Eocene

carbonates (this study and Clarkson et al. (2021), Fig. 6A) when $\Delta^{238}\text{U}_{\text{auth-sw}}$ varies between +0.4 to +0.8‰. The two data points with extremely high $\delta^{238}\text{U}$ values (+0.71 and +0.73‰) likely result from a larger $\Delta^{238}\text{U}_{\text{auth-sw}}$ of $\sim +1.2\text{‰}$. Our model suggests that authigenic accumulation of U(IV) is the predominant factor controlling carbonate $\delta^{238}\text{U}$ with positive isotopic offsets (relative to coeval seawater) during diagenesis, accounting for the general increasing trend of carbonate $\delta^{238}\text{U}$ with U/Ca.

5.4 $\delta^{238}\text{U}$ in calcite is more sensitive to diagenesis than aragonite

Our work and previous studies reveal that $\delta^{238}\text{U}$ and U/Ca in primary calcite is more susceptible to diagenetic alterations as compared to primary aragonite. Specifically, foraminiferal calcite admixed with Mn oxides or organic matter led to a negative shift of $\sim 0.2\text{‰}$ in carbonate $\delta^{238}\text{U}$ from coeval Paleocene-Eocene seawater (Clarkson et al., 2021; Fig. 4 *this study*). Modern microbial calcite deposited under sulfidic bottom waters of the redox-stratified Fayetteville Green Lake (New York, USA) also caused a U isotope fractionation of $\sim +0.6\text{‰}$ relative to the bottom water of this lake (Chen et al., 2021). The Paleocene-Eocene foraminiferal calcite deposited under suboxic to anoxic bottom waters resulted in a U isotopic offset of +0.4 to +0.6‰ relative to contemporaneous seawater (Clarkson et al., 2021). Our data further demonstrates that primary calcite deposited under oxic bottom waters and alongside reducing but non-sulfidic pore water can also lead to positive U isotopic offsets of $0.59 \pm 0.24\text{‰}$ ($N = 24$, 1σ) due to authigenic reductive accumulation of U(IV) in pore water below the sediment-water interface. The average U/Ca in carbonate sediments with $\delta^{238}\text{U}$ values higher than in modern seawater was $1.03 \pm 1.60 \mu\text{mol/mol}$ ($N = 46$, 1σ), which was generally one order of magnitude higher than in primary calcite (predominantly foraminifera with an average value of $0.06 \pm 0.04 \mu\text{mol/mol}$, $N = 48$, 1σ ; Clarkson

et al., 2021; Chen, 2020). Briefly, diagenesis of primary calcite precipitates can result in negative U isotopic offsets ($-0.18 \pm 0.09\text{‰}$, $N = 13$, 1σ) due to Mn oxides and positive offsets ($+0.50 \pm 0.22\text{‰}$, $N = 46$, 1σ) because of authigenic reductive accumulation of U(IV) in sulfidic water columns and below the sediment-water interface. Additionally, these positive offsets generally increased with U/Ca (Fig. 6A), which can be described by the authigenic reductive accumulation model (see Section 5.3.3).

In contrast, modern Bahamian shallow-water platform carbonate sediments that have a predominantly primary aragonitic mineralogy tend to have a tighter range in $\delta^{238}\text{U}$ with a much smaller U isotopic offset of $+0.25 \pm 0.15\text{‰}$ ($N = 162$, 1σ ; Fig. 4B and Fig. 6B) relative to modern seawater (Romaniello et al., 2013; Chen et al., 2018b; Tissot et al., 2018). The mean value of U/Ca in these carbonate sediments was $2.20 \pm 0.95 \mu\text{mol/mol}$ ($N = 162$, 1σ), which was about 3-fold higher than that in primary aragonite (corals and calcareous green algae with an average value of $0.79 \pm 0.46 \mu\text{mol/mol}$, $N = 39$, 1σ) in modern oceans (Romaniello et al., 2013; Chen et al., 2018a, b; Tissot et al., 2018; Livermore et al., 2020). The variation of $\delta^{238}\text{U}$ with U/Ca in these carbonate sediments did not follow the increasing trend (Fig. 6B; $\rho = 0.04$, $p\text{-value} = 0.61$ for spearman correlation) as observed in carbonate sediments that have a primary calcitic mineralogy (Fig. 6A; $\rho = 0.66$, $p\text{-value} < 0.01$).

The more sensitive response of $\delta^{238}\text{U}$ and U/Ca in primary calcite to the influence of diagenesis relative to primary aragonite most likely results from the significantly lower U/Ca in calcite. If we assume that pore water U(VI) reduction below the sediment-water interface can produce $\sim 1.6 \text{ ppm}$ U(IV) during diagenesis, the quantity of U(IV) is about 1 – 2 orders of magnitude greater than that in primary calcite ($0.2 - 30 \text{ ppb}$; e.g., Allen et al., 2016), and approximately 0.7 – 4 times of that in primary aragonite ($0.4 - 2.4 \text{ ppm}$; e.g., Romaniello et al.,

2013; Livermore et al., 2020). As a result, the original U in primary calcite would account for ~ 2% of the total U in carbonate sediments after cementation, whereas U in primary aragonite would be ~ 20 – 40% of the total U in bulk carbonate sediments. Obviously, authigenic reductive accumulation of U(IV) could more easily overprint the original U isotope signature in primary calcite as compared to primary aragonite, producing a general increasing trend of $\delta^{238}\text{U}$ with U/Ca (Fig. 6A) in carbonate sediments that started with a primary calcitic mineralogy.

Similarly, the lower U concentration in primary calcite makes carbonate $\delta^{238}\text{U}$ more susceptible to the effect of Mn oxides than primary aragonite. Ferromanganese crust and nodules in modern oceans typically have U concentrations of ~ 10 ppm (Hein and Koschinsky, 2013), which is about three orders of magnitude larger than in the primary foraminiferal calcite ($\sim 27 \pm 23$ ppb; Russell et al., 2004; Keul et al., 2013; Allen et al., 2016; Chen, 2020). As a result, the admixture of Mn oxides with primary calcite (Clarkson et al., 2021; Herrmann et al., 2018) can easily cause negative shifts in carbonate $\delta^{238}\text{U}$ during carbonate diagenesis. In contrast, primary aragonite and Mn oxides in modern oceans have the same order of magnitude in U concentration, making $\delta^{238}\text{U}$ in carbonate sediments that have a primary aragonitic mineralogy more resistant to diagenetic alterations due to Mn oxides.

In summary, $\delta^{238}\text{U}$ of bulk carbonate sediments dominated by primary calcite grains are more sensitive to diagenesis compared to aragonite-bearing equivalents because calcite typically has significantly lower U concentrations than aragonite. Variations of $\delta^{238}\text{U}$ in bulk carbonate sediments that have a primary calcitic mineralogy more likely reflect the redox state of local early diagenetic environments, to first order, and require careful screening in order to be used as indicators of global seawater U isotope signatures (see the discussion below). Carbonate sediments with low U/Ca that is closer to that of primary calcite are more likely to represent seawater $\delta^{238}\text{U}$

(Fig. 6 A), although carbonate $\delta^{238}\text{U}$ is still likely to be affected by Mn oxides and organic matter that can result in limited negative offsets ($< 0.2\text{‰}$) from coeval seawater.

5.5 Cross-correlations of U/Ca, $\delta^{238}\text{U}$, and traditional diagenetic indicators of carbonates

Our results reveal a positive correlation ($\rho = 0.47$, $p\text{-value} = 0.02$ for spearman correlation) between $\delta^{238}\text{U}$ and U/Ca in carbonate sediments from ODP Hole 871C, whereas these two geochemical signals show statistically insignificant correlations with traditional diagenetic indicators (e.g., $\delta^{13}\text{C}_{\text{carb}}$, $\delta^{18}\text{O}_{\text{carb}}$, Sr/Ca, Mg/Ca, and Mn/Sr) and cerium anomaly (Ce/Ce*) (Fig. 7). Since calcite typically has low U concentration (< 100 ppb), authigenic U(IV) during diagenesis dominates over U in primary calcite and leads to the positive correlation between U/Ca and $\delta^{238}\text{U}$.

Unlike carbonate sediments from ODP Hole 871C, the platform carbonate sediments from the Bahamas show statistically insignificant correlation between U/Ca and $\delta^{238}\text{U}$ and have a predominantly primary aragonitic mineralogy (Chen et al., 2018a; Tissot et al., 2018). This insignificant correlation most likely results from the decoupling of U/Ca from $\delta^{238}\text{U}$ during carbonate mineralogy transformations (*i.e.*, aragonite to calcite transition). Carbonate sediments from the Bahamas have undergone extensive aragonite-to-calcite transformation and significant authigenic enrichments of U(IV) (Chen et al., 2018a; Tissot et al., 2018; Romaniello et al., 2013). Aragonite-to-calcite transformation during meteoric diagenesis of a *Orbicella annularis* coral head from the Pleistocene Key Largo Limestone resulted in $\sim 50\%$ decrease in U/Ca but no changes in $\delta^{238}\text{U}$ values (Chen et al., 2018a). Abiotic calcium carbonate coprecipitation experiments also demonstrated much lower U concentration in aragonite compared to calcite (~ 2200 ppm vs. ~ 350 ppm) but negligible difference in $\delta^{238}\text{U}$ in these two carbonate minerals (Chen et al., 2016). As a result, the decoupling of U/Ca from $\delta^{238}\text{U}$ during aragonite-to-calcite transformation breaks down

the positive correlation between U/Ca and $\delta^{238}\text{U}$ due to authigenic accumulation of U(IV) in diagenetic alteration of pristine aragonite. In short, U/Ca is governed by both carbonate mineralogy and porewater U reduction during diagenesis of carbonate sediments from the Bahamas, whereas $\delta^{238}\text{U}$ in the same carbonates sediments is predominantly controlled by porewater U reduction.

Since $\delta^{238}\text{U}$ in carbonate sediments predominantly depends on porewater U reduction, carbonate $\delta^{238}\text{U}$ from the Bahamas (Chen et al., 2018a; Tissot et al., 2018) and ODP Hole 871C do not show significant correlations with traditional diagenetic indices for changes in carbonate morphology (e.g., recrystallization from aragonite to calcite (Sr/Ca), dolomitization (Mg/Ca)), meteoric diagenesis ($\delta^{13}\text{C}_{\text{carb}}$ and $\delta^{18}\text{O}_{\text{carb}}$), and the extent of diagenetic alterations of carbonates (Mn/Sr). These findings caution against using these traditional diagenetic indicators to argue for the well-preservation of $\delta^{238}\text{U}$ values during carbonate diagenesis.

5.6 Implications for carbonate $\delta^{238}\text{U}$ as a global paleoredox proxy

The higher sensitivity of $\delta^{238}\text{U}$ in primary calcite (relative to primary aragonite) during diagenesis suggests that caution should be exercised when interpreting carbonate $\delta^{238}\text{U}$ data from carbonate sediments that have a primary calcitic mineralogy to reconstruct the past global redox conditions of oceans. It is essential to first identify the original carbonate mineralogy (aragonite or calcite) using geochemical indicators such as Sr/Ca. If the original mineralogy was calcite, it is then crucial to determine the redox state of the local depositional environments using biogeochemical proxies such as cerium anomalies, I/Ca, redox-sensitive elements (Mo, Re, and Mn), and benthic foraminiferal assemblages (e.g., Loubere, 1996; Tostevin et al., 2016; Lu et al., 2010). When primary calcite precipitates were deposited under anoxic bottom waters, the original carbonate $\delta^{238}\text{U}$ would be completely overprinted in bulk sediments by the relatively high U-

bearing diagenetic phases and, consequently, altered to be heavier than coeval seawater thereby only reflecting the local redox conditions (Fig. 6A, Chen et al., 2021; Clarkson et al., 2021). Under oxic depositional conditions, carbonate sediments that have low U/Ca values close to those of primary calcite precipitates ($< 0.10 \mu\text{mol/mol}$, e.g., Russell et al., 2004) most likely capture global seawater $\delta^{238}\text{U}$, whereas carbonate sediments with high U/Ca ($> 0.10 \mu\text{mol/mol}$, *i.e.*, ODP Hole 871C this study) tend to reflect the effects of local diagenetic alterations on $\delta^{238}\text{U}$.

If the original carbonate mineralogy was aragonite, $\delta^{238}\text{U}$ in bulk carbonate sediments (e.g., modern Bahamian shallow-water platform carbonate sediments) would record U isotopic compositions that are close or heavier than coeval seawater $\delta^{238}\text{U}$ after diagenesis (Chen et al., 2018b; Tissot et al., 2018). Since U concentration in aragonite is significantly higher than calcite and comparable to the concentrations achieved through authigenic reductive accumulation of U(IV) during early diagenesis, $\delta^{238}\text{U}$ in bulk carbonate sediments that were originally aragonite in composition are less sensitive to the degree of diagenetic alteration and more likely exhibit consistent positive isotopic offsets from coeval seawater (e.g., $\sim 0.25 \pm 0.15\text{‰}$ in Bahamian carbonate sediments). Thus, we argue that $\delta^{238}\text{U}$ in bulk carbonate sediments that have a primary aragonitic mineralogy are more likely to record changes in coeval seawater $\delta^{238}\text{U}$ and global oceanic redox conditions.

6. Conclusions

We observed larger positive and negative fluctuations of carbonate $\delta^{238}\text{U}$ values (relative to modern seawater) in shallow-water Paleocene-Eocene carbonate sediments that have a primary calcitic mineralogy and deposited under oxic bottom waters, suggesting that $\delta^{238}\text{U}$ in primary calcite is more susceptible to carbonate diagenesis compared to primary aragonite. Our work

implies that variations of $\delta^{238}\text{U}$ in carbonate sediments that have a primary calcitic mineralogy more likely reflects the redox state of pore waters. These carbonate sediments that have U/Ca values close to primary calcite more likely record and preserve seawater $\delta^{238}\text{U}$. Thus, it is essential to identify the original carbonate mineralogy (aragonite or calcite) and constrain the local depositional conditions of carbonates when interpreting carbonate $\delta^{238}\text{U}$ data and applying it to reconstruct the global redox conditions of oceans through time.

Acknowledgements

This work was supported by the U.S. National Science Foundation (Grant OCE-0952394) and the NASA Exobiology Program. The authors are grateful to two anonymous reviewers for helpful comments on the manuscript.

Appendix A. Supplementary data

Supplementary data to this article can be found online at ...

References

- Abshire M. L., Romaniello S. J., Kuzminov A. M., Cofrancesco J., Severmann S. and Riedinger N. (2020) Uranium isotopes as a proxy for primary depositional redox conditions in organic-rich marine systems. *Earth Planet. Sci. Lett.* **529**, 115878.
- Algeo T. J. and Tribovillard N. (2009) Environmental analysis of paleoceanographic systems based on molybdenum-uranium covariation. *Chem. Geol.* **268**, 211–225.
- Allen K. A., Honisch B., Eggins S. M., Haynes L. L., Rosenthal Y. and Yu J. (2016) Trace element proxies for surface ocean conditions: A synthesis of culture calibrations with planktic foraminifera. *Geochim. Cosmochim. Acta* **193**, 197–221.
- Anbar A. D. and Rouxel O. (2007) Metal stable isotopes in paleoceanography. *Annu. Rev. Earth Planet. Sci.* **35**, 717–746.
- Andersen M. B., Romaniello S., Vance D., Little S. H., Herdman R. and Lyons T. W. (2014) A

565 modern framework for the interpretation of $^{238}\text{U}/^{235}\text{U}$ in studies of ancient ocean redox. *Earth*
566 *Planet. Sci. Lett.* **400**, 184–194.

567 Andersen M. B., Stirling C. H. and Weyer S. (2017) Uranium isotope fractionation. *Rev. Mineral.*
568 *Geochemistry* **82**, 799–850.

569 Basu A., Sanford R. A., Johnson T. M., Lundstrom C. C. and Löffler F. E. (2014) Uranium isotopic
570 fractionation factors during U(VI) reduction by bacterial isolates. *Geochim. Cosmochim. Acta*
571 **136**, 100–113.

572 Basu A., Wanner C., Johnson T. M., Lundstrom C. C., Sanford R. A., Sonnenthal E. L., Boyanov
573 M. I. and Kemner K. M. (2020) Microbial U Isotope Fractionation Depends on the U(VI)
574 Reduction Rate. *Environ. Sci. Technol.* **54**, 2295–2303.

575 Berner R. A., VandenBrooks J. M. and Ward P. D. (2007) Oxygen and evolution. *Science* **316**,
576 557–558.

577 Brennecka G. A., Herrmann A. D., Algeo T. J. and Anbar A. D. (2011) Rapid expansion of oceanic
578 anoxia immediately before the end-Permian mass extinction. *Proc. Natl. Acad. Sci.* **108**,
579 17631–17634.

580 Brennecka G., Wasylenki L. E., Weyer S. and Anbar A. D. (2011) Uranium isotope fractionation
581 during adsorption to manganese oxides. *Environ. Sci. Technol.* **45**, 1370–1375.

582 Chen X. (2020) Aqueous uranium speciation on U/Ca in foraminiferal calcite: The importance of
583 minor species— $\text{UO}_2(\text{CO}_3)_2^{2-}$. *ACS Earth Sp. Chem.* **4**, 2050–2060.

584 Chen X., Romaniello S. J. and Anbar A. D. (2017) Uranium isotope fractionation induced by
585 aqueous speciation: Implications for U isotopes in marine CaCO_3 as a paleoredox proxy.
586 *Geochim. Cosmochim. Acta* **215**, 162–172.

587 Chen X., Romaniello S. J., Herrmann A. D., Hardisty D., Gill B. C. and Anbar A. D. (2018a)
588 Diagenetic effects on uranium isotope fractionation in carbonate sediments from the
589 Bahamas. *Geochim. Cosmochim. Acta* **237**, 294–311.

590 Chen X., Romaniello S. J., Herrmann A. D., Samankassou E. and Anbar A. D. (2018b) Biological
591 effects on uranium isotope fractionation ($^{238}\text{U}/^{235}\text{U}$) in primary biogenic carbonates.
592 *Geochim. Cosmochim. Acta* **240**, 1–10.

593 Chen X., Romaniello S. J., Herrmann A. D., Wasylenki L. E. and Anbar A. D. (2016) Uranium
594 isotope fractionation during coprecipitation with aragonite and calcite. *Geochim. Cosmochim.*
595 *Acta* **188**, 189–207.

596 Chen X., Zheng W. and Anbar A. D. (2020) Uranium isotope fractionation ($^{238}\text{U}/^{235}\text{U}$) during
597 U(VI) Uptake by Freshwater Plankton. *Environ. Sci. Technol.* **54**, 2744–2752.

598 Chen X., Romaniello S. J., McCormick M., Sherry A., Havig J. R., Zheng W. and Anbar A. D.
599 (2021) Anoxic depositional overprinting of $^{238}\text{U}/^{235}\text{U}$ in calcite: When do carbonates tell black

shale tales? *Geology* <http://doi.org/10.1130/G48949.1>.

Cheng K., Elrick M. and Romaniello S. J. (2020) Early Mississippian ocean anoxia triggered organic carbon burial and late Paleozoic cooling: Evidence from uranium isotopes recorded in marine limestone. *Geology* **48**, 363–367.

Chun C. O. J., Delaney M. L. and Zachos J. C. (2010) Paleoredox changes across the Paleocene-Eocene thermal maximum, Walvis Ridge (ODP Sites 1262, 1263, and 1266): Evidence from Mn and U enrichment factors. *Paleoceanography* **25**, 1–13.

Clarkson M. O., Lenton T. M., Andersen M. B., Bagard M. L., Dickson A. J. and Vance D. (2021) Upper limits on the extent of seafloor anoxia during the PETM from uranium isotopes. *Nat. Commun.* **12**, 399.

Dang D. H., Novotnik B., Wang W., Georg R. B. and Evans R. D. (2016) Uranium isotope fractionation during adsorption, (co)precipitation, and biotic reduction. *Environ. Sci. Technol.* **50**, 12695–12704.

del Rey Á., Havsteen J. C., Bizzarro M. and Dahl T. W. (2020) Untangling the diagenetic history of uranium isotopes in marine carbonates: A case study tracing the $\delta^{238}\text{U}$ composition of late Silurian oceans using calcitic brachiopod shells. *Geochim. Cosmochim. Acta* **287**, 93–110.

Dunk R. M., Mills R. A. and Jenkins W. J. (2002) A reevaluation of the oceanic uranium budget for the Holocene. *Chem. Geol.* **190**, 45–67.

Elrick M., Polyak V., Algeo T. J., Romaniello S., Asmerom Y., Herrmann A. D., Anbar A. D., Zhao L. and Chen Z. Q. (2017) Global-ocean redox variation during the middle-late Permian through Early Triassic based on uranium isotope and Th/U trends of marine carbonates. *Geology* **45**, 163–166.

Fan H., Ostrander C. M., Auro M., Wen H. and Nielsen S. G. (2021) Vanadium isotope evidence for expansive ocean euxinia during the appearance of early Ediacara biota. *Earth Planet. Sci. Lett.* **567**, 117007.

Fenchel T. and Finlay B. J. (1994) The evolution of life without oxygen. *Am. Sci.* **82**, 22–29.

Gilleaudeau G. J., Romaniello S. J., Luo G., Kaufman A. J., Zhang F., Klæbe R. M., Kah L. C., Azmy K., Bartley J. K., Zheng W., Knoll A. H. and Anbar A. D. (2019) Uranium isotope evidence for limited euxinia in mid-Proterozoic oceans. *Earth Planet. Sci. Lett.* **521**, 150–157.

Haley B. A., Klinkhammer G. P. and McManus J. (2004) Rare earth elements in pore waters of marine sediments. *Geochim. Cosmochim. Acta* **68**, 1265–1279.

Hein J. R. and Koschinsky A. (2013) Deep-Ocean Ferromanganese Crusts and Nodules. In *The Treatise on Geochemistry*; Scott, S., Ed.; Elsevier: Amsterdam, The Netherlands.

Jemison N. E., Johnson T. M., Shiel A. E. and Lundstrom C. C. (2016) Uranium isotopic

635 fractionation induced by U(VI) adsorption onto common aquifer minerals. *Environ. Sci.*
636 *Technol.* **50**, 12232–12240.

637 Jones C., Canfield D. E., Sweeten B., Treusch A. H., Forth M., Ward L. M. and Mills D. B. (2014)
638 Oxygen requirements of the earliest animals. *Proc. Natl. Acad. Sci.* **111**, 4168–4172.

639 Keul N., Langer G., De Nooijer L. J., Nehrke G., Reichart G. J. and Bijma J. (2013) Incorporation
640 of uranium in benthic foraminiferal calcite reflects seawater carbonate ion concentration.
641 *Geochemistry, Geophys. Geosystems* **14**, 102–111.

642 Ku T.-L., Mathieu G. G. and Knauss K. G. (1977) Uranium in open ocean: concentration and
643 isotopic composition. *Deep Sea Res.* **24**, 1005–1017. Available at:
644 <https://www.sciencedirect.com/science/article/pii/0146629177905719>.

645 Lau K. V., Maher K., Altiner D., Kelley B. M., Kump L. R., Lehrmann D. J., Silva-Tamayo J. C.,
646 Weaver K. L., Yu M. and Payne J. L. (2016) Marine anoxia and delayed Earth system
647 recovery after the end-Permian extinction. *Proc. Natl. Acad. Sci.* **113**, 2360–2365.

648 Ling H.-F., Chen X., Li D., Wang D., Shields-Zhou G. A. and Zhu M. (2013) Cerium anomaly
649 variations in Ediacaran–earliest Cambrian carbonates from the Yangtze Gorges area, South
650 China: Implications for oxygenation of coeval shallow seawater. *Precambrian Res.* **225**, 110–
651 127.

652 Livermore B. D., Dahl T. W., Bizzarro M. and Connelly J. N. (2020) Uranium isotope
653 compositions of biogenic carbonates – Implications for U uptake in shells and the application
654 of the paleo-ocean oxygenation proxy. *Geochim. Cosmochim. Acta* **287**, 50–64.

655 Loubere P. (1996) The surface ocean productivity and bottom water oxygen signals in deep water
656 benthic foraminiferal assemblages. *Mar. Micropaleontol.* **28**, 247–261.

657 Lu Z., Jenkyns H. C. and Rickaby R. E. M. (2010) Iodine to calcium ratios in marine carbonate as
658 a paleo-redox proxy during oceanic anoxic events. *Geology* **38**, 1107–1110.

659 Lyons T. W., Anbar A. D., Severmann S., Scott C. and Gill B. C. (2009) Tracking euxinia in the
660 ancient ocean: A multiproxy perspective and Proterozoic case study. *Annu. Rev. Earth Planet.*
661 *Sci.* **37**, 507–534.

662 Mills D. B., Ward L. M., Jones C. A., Sweeten B., Forth M., Treusch A. H. and Canfield D. E.
663 (2014) Oxygen requirements of the earliest animals. *Proc. Natl. Acad. Sci. U. S. A.* **111**, 4168–
664 4172.

665 Ogg J. G., Camoin G. F. and Arnaud Vanneau A. (1995) Limalok Guyot: Depositional history of
666 the carbonate platform from downhole logs at Site 871 (Lagoon). in Haggerty, J. A., et al.,
667 eds., Proceedings of the Ocean Drilling Program, Scientific results, Volume 144: College
668 Station, Texas, Ocean Drilling Program, p. 233–235, doi:10.2973/odp/proc/sr.144.042.1995.

669 Premoli Silva. I., Haggerty. J., Rack. F., and the Shipboard Scientific Party, 1993, Proceedings of
670 the Ocean Drilling Program, Scientific results, Volume 144: College Station, Texas, Ocean

671 Drilling Program, p. 233–235, doi:10.2973/odp.proc.ir.144.1993.

672 Pufahl P. K. and Hiatt E. E. (2012) Oxygenation of the Earth's atmosphere ocean system: A review
 673 of physical and chemical sedimentologic responses. *Mar. Pet. Geol.* **32**, 1–20. Available at:
 674 <http://dx.doi.org/10.1016/j.marpetgeo.2011.12.002>.

675 Reeder R. J., Nuget M., Lambie G. M., Tait C. D. and Morris D. E. (2000) Uranyl incorporation
 676 into calcite and aragonite XAFS and luminescence studies. *Environ. Sci. Technol.* **34**, 638–
 677 644.

678 Reinhard C. T., Planavsky N. J., Olson S. L., Lyons T. W. and Erwin D. H. (2016) Earth's oxygen
 679 cycle and the evolution of animal life. *Proc. Natl. Acad. Sci. U. S. A.* **113**, 8933–8938.

680 Remmelzwaal S. R. C., Dixon S., Parkinson I. J., Schmidt D. N., Monteiro F. M., Sexton P., Fehr
 681 M. A., Peacock C., Donnadieu Y. and James R. H. (2019) Investigating ocean deoxygenation
 682 during the PETM through the Cr isotopic signature of foraminifera. *Paleoceanogr.*
 683 *Paleoclimatology* **34**, 917–929.

684 Robinson S. A. (2011) Shallow-water carbonate record of the Paleocene-Eocene Thermal
 685 maximum from a Pacific Ocean Guyot. *Geology* **39**, 51–54.

686 Russell A. D., Hönisch B., Spero H. J. and Lea D. W. (2004) Effects of seawater carbonate ion
 687 concentration and temperature on shell U, Mg, and Sr in cultured planktonic foraminifera.
 688 *Geochim. Cosmochim. Acta* **68**, 4347–4361.

689 Scholle P. A. and Ulmer-Scholle D. S. (2003) A color guide to the petrography of carbonate rocks:
 690 Grains, textures, porosity, and diagenesis, AAPG Memoir, 77, 1–477.

691 Stirling C. H., Andersen M. B., Potter E. K. and Halliday A. N. (2007) Low-temperature isotopic
 692 fractionation of uranium. *Earth Planet. Sci. Lett.* **264**, 208–225.

693 Stirling C. H., Andersen M. B., Warthmann R. and Halliday A. N. (2015) Isotope fractionation of
 694 ^{238}U and ^{235}U during biologically-mediated uranium reduction. *Geochim. Cosmochim. Acta*
 695 **163**, 200–218.

696 Stylo M., Neubert N., Wang Y., Monga N., Romaniello S. J., Weyer S. and Bernier-Latmani R.
 697 (2015) Uranium isotopes fingerprint biotic reduction. *Proc. Natl. Acad. Sci.* **112**, 5619–5624.

698 Tissot F. L. H., Chen C., Go B. M., Naziemiec M., Healy G., Bekker A., Swart P. K. and Dauphas
 699 N. (2018) Controls of eustasy and diagenesis on the $^{238}\text{U}/^{235}\text{U}$ of carbonates and evolution of
 700 the seawater ($^{234}\text{U}/^{238}\text{U}$) during the last 1.4 Myr. *Geochim. Cosmochim. Acta* **242**, 233–265.

701 Tissot F. L. H. and Dauphas N. (2015) Uranium isotopic compositions of the crust and ocean: Age
 702 corrections, U budget and global extent of modern anoxia. *Geochim. Cosmochim. Acta* **167**,
 703 113–143.

704 Tostevin R. (2018) Uranium isotope evidence for an expansion of anoxia in terminal Ediacaran
 705 oceans. *Earth Planet. Sci. Lett.* **506**, 104–112.

706 Tostevin R., Shields G. A., Tarbuck G. M., He T., Clarkson M. O. and Wood R. A. (2016) Effective
707 use of cerium anomalies as a redox proxy in carbonate-dominated marine settings. *Chem.*
708 *Geol.* **438**, 146–162.

709 Verbruggen A., Alonso-Munoz A., Eykens R., Kehoe F., Kuhen H., Richter S. and Arbegbe Y.
710 (2008) Preparation and certification of IRMM-3636, IRMM-3636a and IRMM-3636b. *Inst.*
711 *Ref. Mater. Meas.*, 28.

712 Wang X., Johnson T. M. and Lundstrom C. C. (2015) Low temperature equilibrium isotope
713 fractionation and isotope exchange kinetics between U(IV) and U(VI). *Geochim. Cosmochim.*
714 *Acta* **158**, 262–275.

715 Wang X., Planavsky N. J., Reinhard C. T., Hein J. R. and Johnson T. M. (2016) A cenozoic
716 seawater redox record derived from $^{238}\text{U}/^{235}\text{U}$ in ferromanganese crusts. *Am. J. Sci.* **315**,
717 64–83.

718 Watkins D. K., Silva I. P. and Erba E. (1995) Cretaceous and Paleogene manganese-encrusted
719 hardgrounds from central Pacific guyots. Proc. Ocean Drill. Program, 144 Sci. Results.
720 <http://doi.org/10.2937/odp.proc.sr.144.017.1995>.

721 Wei G.-Y., Chen X., Wei W., Li D., Ling H.-F., Planavsky N. J. and Tarhan L. G. (2018) Marine
722 redox fluctuation as a potential trigger for the Cambrian explosion. *Geology* **46**, 587–590.

723 Weyer S., Anbar A. D., Gerdes A., Gordon G. W., Algeo T. J. and Boyle E. A. (2008) Natural
724 fractionation of $^{238}\text{U}/^{235}\text{U}$. *Geochim. Cosmochim. Acta* **72**, 345–359.

725 White D. A., Elrick M., Romaniello S. and Zhang F. (2018) Global seawater redox trends during
726 the Late Devonian mass extinction detected using U isotopes of marine limestones. *Earth*
727 *Planet. Sci. Lett.* **503**, 68–77.

728 Wilson P. A., Jenkyns H. C., Elderfield H., and Larson R. L. (1998) The paradox of drowned
729 carbonate platforms and the origin of Cretaceous Pacific guyots. *Nature* **392**, 889–894.

730 Wyatt J. L., Quinn T. M. and Davies G. R. (1995) Preliminary investigation of the petrography
731 and geochemistry of limestones at Limalok and Wodejebato Guyots (Sites 871 and 874),
732 Republic of the Marshall Islands. in Haggerty J. A., et al., eds., Proceedings of the Ocean
733 Drilling Program, Scientific results, Volume 144: College Station, Texas, Ocean Drilling
734 Program, p. 429–437, doi:10.2973/odp.proc.sr.144.042.1995.

735 Yao W., Paytan A. and Wortmann U. G. (2018) Large-scale ocean deoxygenation during the
736 Paleocene-Eocene Thermal Maximum. *Science* **361**, 804–806.

737 Zeebe R. E. and Tyrrell T. (2019) History of carbonate ion concentration over the last 100 million
738 years II: Revised calculations and new data. *Geochim. Cosmochim. Acta.* **257**, 373–392.

739 Zhang F., Xiao S., Kendall B., Romaniello S. J., Cui H., Meyer M., Gilleaudeau G. J., Kaufman
740 A. J. and Anbar A. D. (2018) Extensive marine anoxia during the terminal ediacaran period.
741 *Sci. Adv.* **4**, 1–12.

742 Zhou X., Thomas E., Rickaby R. E. M., Winguth A. M. E., Lu Z. and Zhou xiaoli (2014) I/Ca
743 evidence for upper ocean deoxygenation during the PETM. *Paleoceanography* **29**, 964–975.

744 Zhou X., Thomas E., Winguth A. M. E., Ridgwell A., Scher H., Hoogakker B. A. A., Rickaby R.
745 E. M. and Lu Z. (2016) Expanded oxygen minimum zones during the late Paleocene-early
746 Eocene: Hints from multiproxy comparison and ocean modeling. *Paleoceanography* **31**,
747 1532–1546.

748

749

750

Figure Captions

Figure 1. (A) Paleogeographic reconstruction of 56 Ma (www.odsni.de) with ODP site 871 marked (B) and contoured bathymetry of Limalok Guyot and ODP Site 871 (from Premoli Silva et al., 1993). The contour interval in panel B is 250 m.

Figure 2. Abundance of redox-sensitive elements V (A), Mo (B), Re (C) and U (D), and Ce anomaly (Ce/Ce^* , E) in shallow-water carbonates from Hole 871C. The stratigraphy is based on benthic forams (Premoli Silva et al., 1993). The dashed blue line represents $Ce/Ce^* = 0.5$. When Ce/Ce^* is below 0.5, it indicates bottom waters are oxic (Haley et al., 2004).

Figure 3. $\delta^{13}C_{carb}$ (A), $\delta^{18}O_{carb}$ (B), U concentration (C), and $\delta^{238}U$ (D) in shallow-water carbonate sediments from ODP Hole 871C. High-resolution $\delta^{238}U$ in carbonates over the PETM from ODP cores 144-871C-23R and -22R (E). The blue dashed line represents $\delta^{238}U$ of modern seawater (-0.39‰ ; Andersen et al., 2015; Tissot and Dauphas, 2015). ‘mbsf’ stands for meters below seafloor. The carbon and oxygen isotope data are from Robinson (2011). The error bars represent twice standard deviations of the sample or the long-term reproducibility of the reference standard CRM-145a, whichever is larger.

Figure 4. Cross plot of carbonate $\delta^{238}U$ versus U/Ca in carbonate sediments (ODP Hole 871C) derived mainly from primary biogenic calcite. The horizontal gray band represent the seawater $\delta^{238}U$ value ($-0.392 \pm 0.005\text{‰}$; Tissot et al., 2015). The error bars are the twice standard deviation of replicate measurements of each sample or the long-term reproducibility the reference standard CRM-145a, whichever is larger. The data for Spearman correlation only consider samples with $\delta^{238}U$ values higher than modern seawater.

Figure 5. Histograms of $\delta^{238}U$ in primary biogenic calcite (yellow; brachiopods, red algae, and echinoderm) and aragonite (red; corals and green algae) and shallow-water carbonate sediments derived mainly from biogenic calcite (‘Calcite-origin’, grey; this study) and aragonite (‘Aragonite-origin’, blue) in modern oceans (Chen et al., 2018b, 2018b; Romaniello et al., 2013; Tissot et al., 2018; Livermore et al., 2020). The dashed pink lines represent seawater $\delta^{238}U$. The arrows stand for the magnitude of the isotopic offsets between carbonate sediments and modern seawater.

Figure 6. Cross plots of carbonate $\delta^{238}U$ versus U/Ca in primary calcite (orange symbols; brachiopods, corals, red algae, echinoderm, and foraminifera) and aragonite (gray symbols; corals and calcareous green algae), and carbonate sediments that have a primary calcitic (‘Calcite-origin’, blue and pink symbols, A) and aragonitic (‘Aragonite-origin’, white symbols, B) mineralogy in modern oceans (Chen et al., (2018a, 2018b), Livermore et al., (2020); Romaniello et al., (2013); Clarkson et al., (2021); Tissot et al., (2018)). The horizontal gray band represent the seawater $\delta^{238}U$ value ($-0.392 \pm 0.005\text{‰}$; Tissot et al., 2015). The error bars are 2 SD of samples. The gray areas in panels A and B represent the range of carbonate $\delta^{238}U$ based on the authigenic enrichment model

in Section 5.3.2 when the isotope fractionation during U reduction ranges between +0.4 and +0.8‰ when the U/Ca ratios in primary calcite and aragonite vary between ~ 0.03 and 0.12 μmol/mol and between ~ 0.2 and 1.0 μmol/mol, respectively. The spearman correlation coefficient ρ and p -value are listed in panels A and B. Only carbonate samples that have $\delta^{238}\text{U}$ values higher than modern seawater were used for spearman correlation analysis.

Figure 7. Cross plots of U/Ca, $\delta^{238}\text{U}$, Ce/Ce*, and diagenetic parameters (Sr/Ca, Mg/Ca, Mn/Sr, $\delta^{13}\text{C}_{\text{carb}}$, and $\delta^{18}\text{O}_{\text{carb}}$) for ODP Hole 871C. Spearman's rank values (ρ , p -value) are displayed in each panel. Panels with full colors indicates statistically significant correlations (*i.e.*, p -value < 0.05); panels with transparent colors represent non-significant correlations. Blue and red symbols represent carbonate $\delta^{238}\text{U}$ values higher and lower than modern seawater $\delta^{238}\text{U}$ (−0.39‰; Tissot and Dauphas, 2015). Samples with $\delta^{238}\text{U}$ values lower than modern seawater were not included in spearman correlation analysis. The $\delta^{13}\text{C}_{\text{carb}}$ and $\delta^{18}\text{O}_{\text{carb}}$ data were from Robinson (2011).

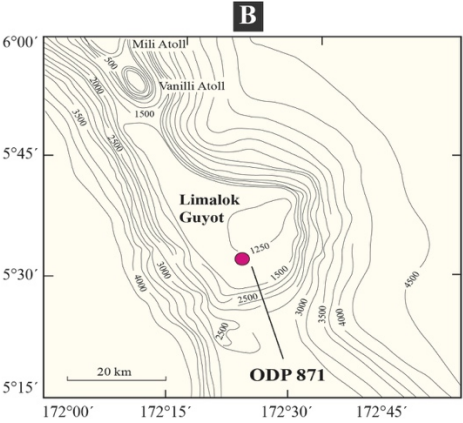
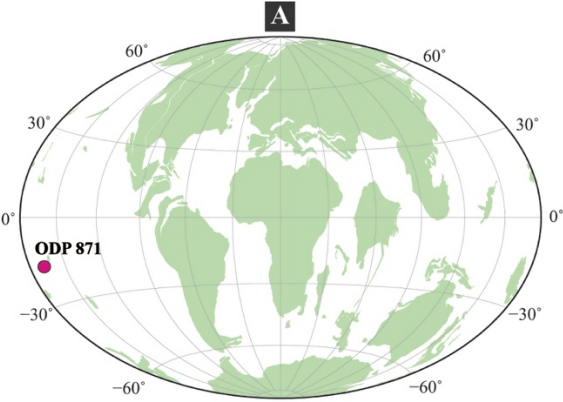
811 Table 1. Summary of elemental ratios (Sr/Ca, Mg/Ca, U/Ca, and Mn/Sr), stable isotopic
812 compositions ($\delta^{13}\text{C}$, $\delta^{18}\text{O}$, and $\delta^{238}\text{U}$), and cerium anomaly in ODP Hole 871C

| Sample ID | Depth mbsf | $\delta^{13}\text{C}$ ‰ | $\delta^{18}\text{O}$ ‰ | $\delta^{238}\text{U}$ ‰ | 2 SD ‰ | Sr/Ca mmol/mol | Mg/Ca mmol/mol | Mn/Sr mol/mol | U/Ca mmol/mol | Ce/Ce* |
|--------------|---------------|----------------------------|----------------------------|-----------------------------|-----------|-------------------|-------------------|------------------|------------------|--------|
| LIM 90 | 153.00 | 1.7 | -1.6 | 0.47 | 0.10 | 0.37 | 24.26 | 0.18 | 2.18 | 0.34 |
| LIM 103 | 172.60 | 0.8 | -2.1 | -0.19 | 0.13 | 0.34 | 24.30 | 0.07 | 0.09 | 0.28 |
| LIM 110 | 191.55 | 0.7 | -2.2 | 0.13 | 0.10 | 0.22 | 22.34 | 0.04 | 0.39 | 0.35 |
| LIM 115 | 201.35 | -0.8 | -3.8 | 0.22 | 0.10 | 0.28 | 26.78 | 0.08 | 1.01 | 0.36 |
| LIM 123 | 211.00 | 0.6 | -4.2 | 0.26 | 0.10 | 0.22 | 26.05 | 0.04 | 0.72 | 0.40 |
| LIM 132 | 249.70 | 1.0 | -1.6 | 0.35 | 0.13 | 0.27 | 18.22 | 0.01 | 0.27 | 0.29 |
| LIM 2 | 268.85 | -0.2 | -3.8 | 0.07 | 0.10 | 0.21 | 16.20 | 0.02 | 0.31 | 0.27 |
| LIM 5 | 278.11 | -0.1 | -3.6 | -0.10 | 0.10 | 0.22 | 20.05 | 0.02 | 0.28 | 0.30 |
| LIM 9 | 297.25 | -0.2 | -3.8 | 0.26 | 0.10 | 0.31 | 24.36 | 0.01 | 0.60 | 0.26 |
| LIM 28 | 317.25 | 1.5 | -0.9 | -0.59 | 0.11 | 0.27 | 22.83 | 0.02 | 5.63 | 0.19 |
| LIM 47 | 326.21 | 1.0 | -0.8 | 0.47 | 0.11 | 0.28 | 22.24 | 0.01 | 3.37 | 0.21 |
| LIM 48 | 326.26 | 1.4 | 0.4 | -0.47 | 0.10 | 0.28 | 23.10 | 0.02 | 5.88 | 0.19 |
| LIM 49 | 326.32 | 1.0 | -1.3 | -0.47 | 0.11 | 0.29 | 24.01 | 0.03 | 4.03 | 0.20 |
| LIM 50 | 326.37 | 1.3 | -1.1 | 0.64 | 0.10 | 0.29 | 20.14 | 0.02 | 9.92 | 0.19 |
| LIM 51 | 326.42 | 0.7 | -1.2 | -0.69 | 0.10 | 0.20 | 21.91 | 0.03 | 4.55 | 0.23 |
| LIM 53 | 335.80 | 1.5 | -1.7 | -0.49 | 0.10 | 0.26 | 22.89 | 0.03 | 4.88 | 0.23 |
| LIM 54 | 335.85 | -1.3 | -3.8 | -0.02 | 0.10 | 0.35 | 22.42 | 0.01 | 0.81 | 0.19 |
| LIM 56 | 335.95 | -0.5 | -2.6 | -0.01 | 0.11 | 0.21 | 23.32 | 0.01 | 0.38 | 0.23 |
| LIM 60 | 336.15 | 0.9 | 0.8 | 0.38 | 0.11 | 0.22 | 21.20 | 0.01 | 0.18 | 0.25 |
| LIM 63 | 336.30 | 1.6 | -1.2 | 0.71 | 0.10 | 0.27 | 24.65 | 0.01 | 4.09 | 0.19 |
| LIM 66 | 345.40 | 0.8 | -2.3 | -0.09 | 0.10 | 0.21 | 18.90 | 0.01 | 0.96 | 0.19 |
| LIM 67 | 355.10 | 1.8 | -0.4 | 0.33 | 0.12 | 0.17 | 18.70 | 0.04 | 0.35 | 0.22 |
| LIM 70 | 355.25 | 1.6 | -1.2 | 0.03 | 0.11 | 0.20 | 20.02 | 0.03 | 0.20 | 0.24 |
| LIM 73 | 364.75 | 1.8 | -1.1 | 0.03 | 0.10 | 0.25 | 21.19 | 0.04 | 0.39 | 0.23 |
| LIM 75 | 374.35 | 1.8 | -1.2 | 0.39 | 0.10 | 0.23 | 18.53 | 0.03 | 2.51 | 0.17 |
| LIM 155 | 384.70 | 1.8 | -0.7 | 0.17 | 0.11 | 0.25 | 19.32 | 0.06 | 1.27 | 0.23 |
| LIM 163 | 393.50 | 1.4 | -1.1 | 0.25 | 0.11 | 0.26 | 21.64 | 0.14 | 0.23 | 0.30 |
| LIM 179 | 404.00 | 1.9 | -0.9 | 0.03 | 0.11 | 0.25 | 19.93 | 0.06 | 2.17 | 0.28 |
| LIM 185 | 412.90 | 1.2 | -1.1 | 0.39 | 0.10 | 0.29 | 21.33 | 0.01 | 0.32 | 0.23 |

813 Note: $\delta^{13}\text{C}$ and $\delta^{18}\text{O}$ were from Robinson (2011).

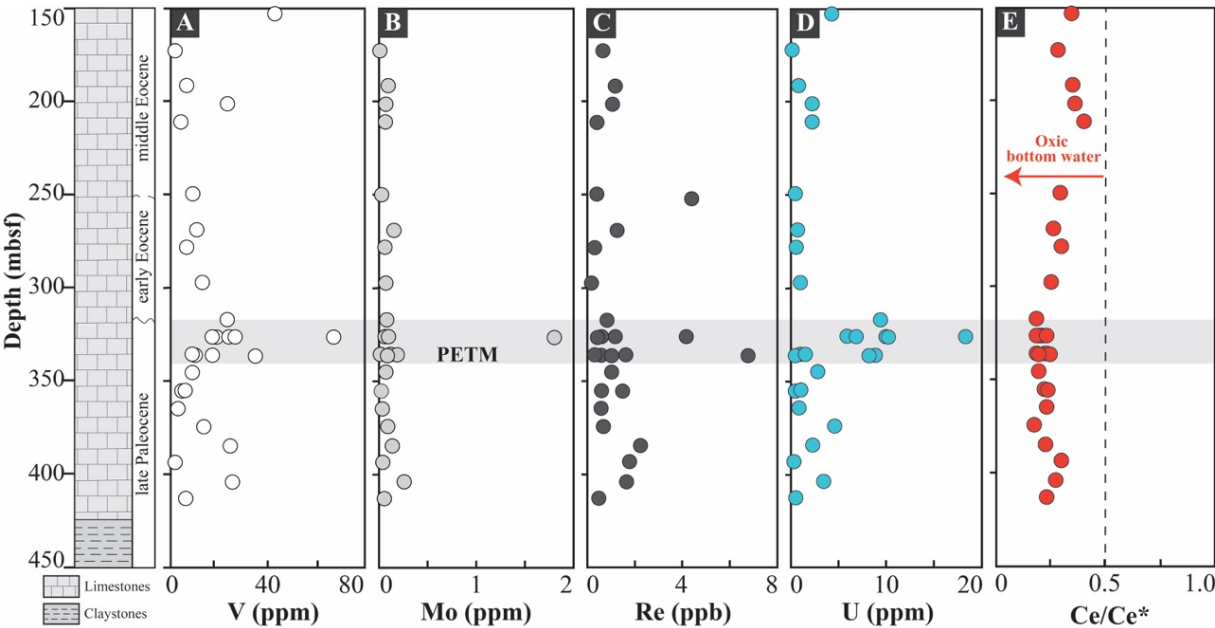
814

815 **Figure 1.**



816

817 **Figure 2.**



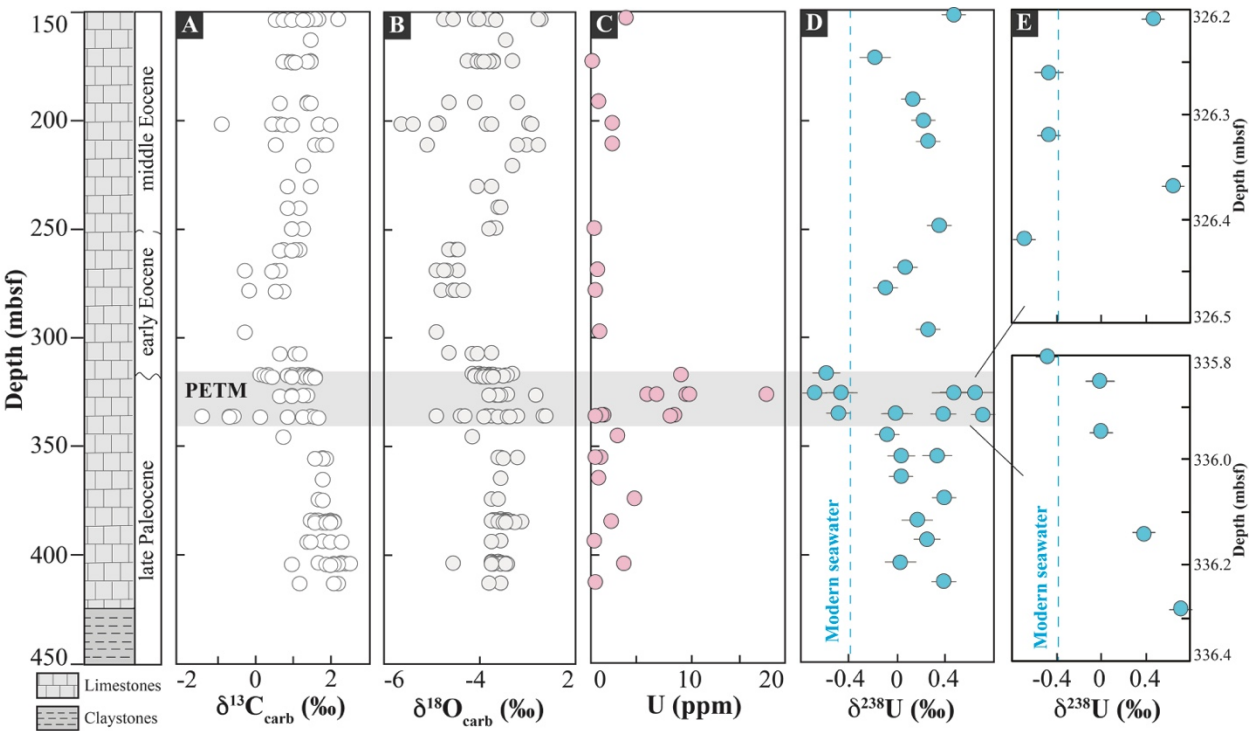
818

819

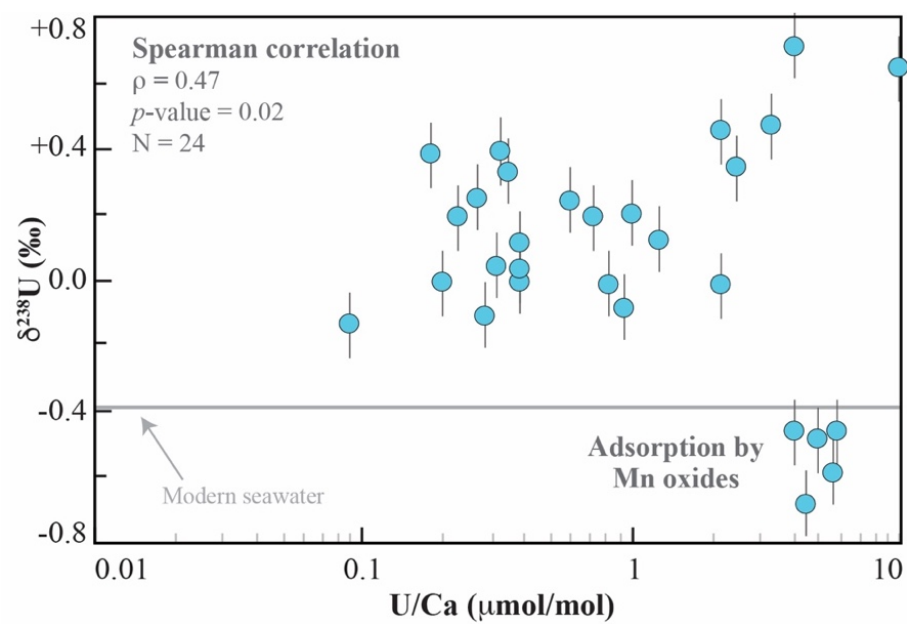
820

821

822 **Figure 3.**



826 **Figure 4.**

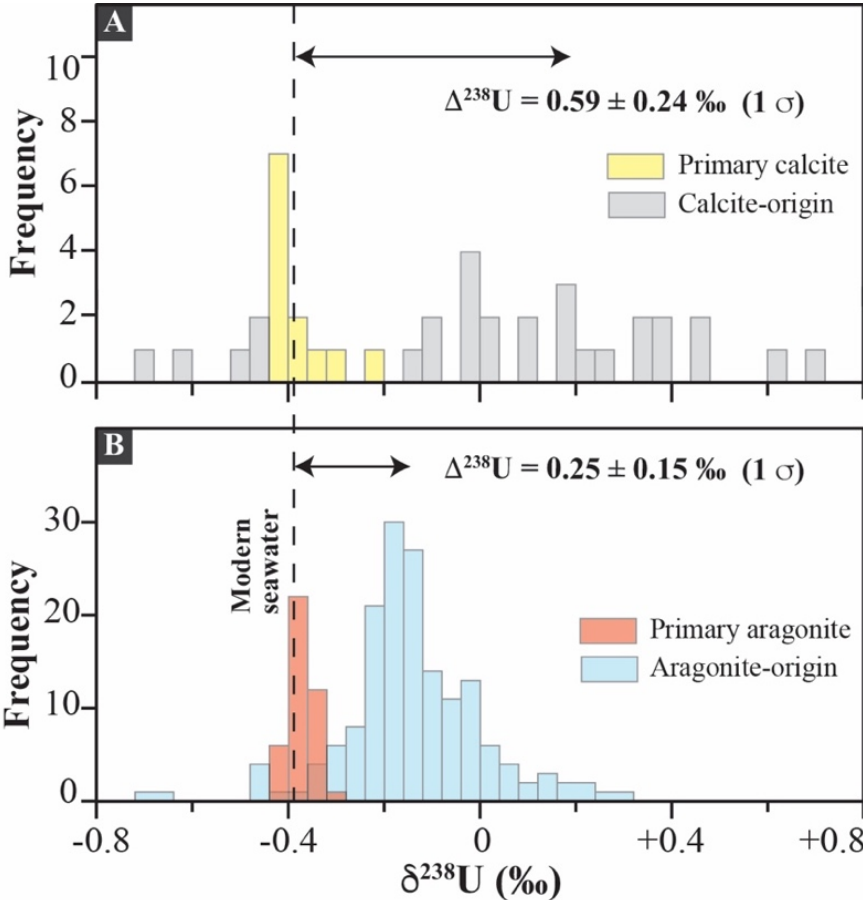


827

828

829

830 **Figure 5.**

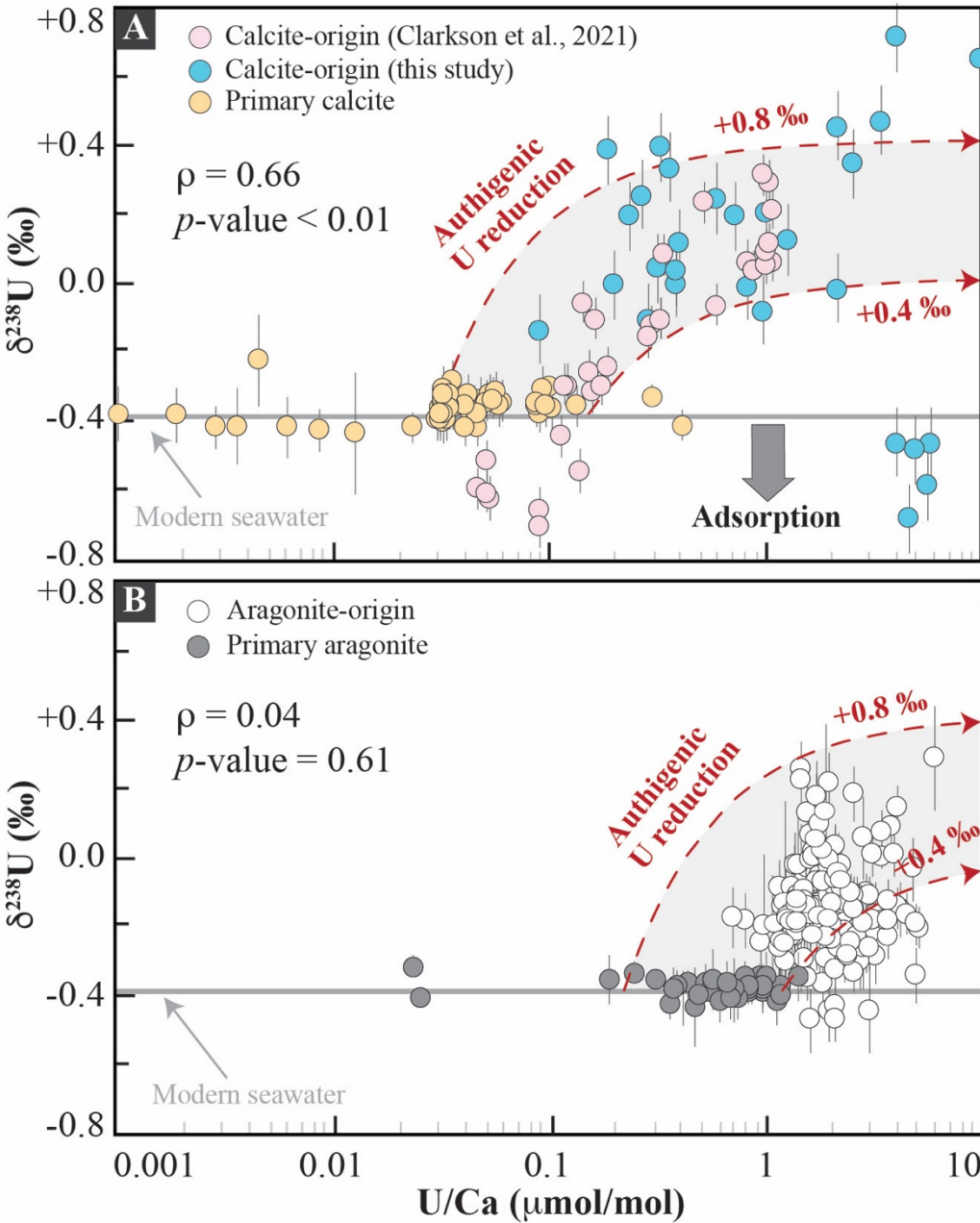


831

832

833

834 **Figure 6.**



835

836

837 **Figure 7**

